AD-A085 978 CALSPAN ADVANCED TECHNOLOGY CENTER BUFFALO NY AERODYN--ETC F/G 20/4
NUMERICAL STUDIES OF THE RADIATION CONDITION AT THE INLET OF A --ETC(U)
APR 80 W J RAE, G F HOMICZ N00019-78-C-0603
UNCLASSIFIED CALSPAN-6432-A-1 NL

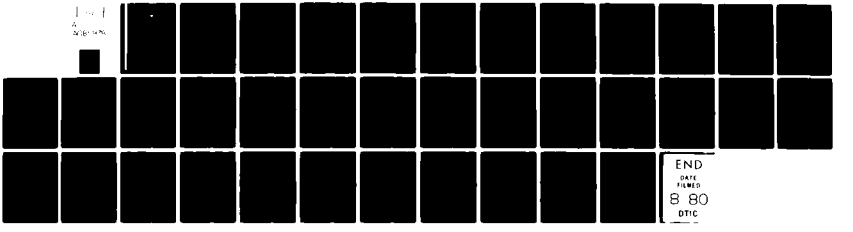

END
DATE FILMED
8 80
DTIC

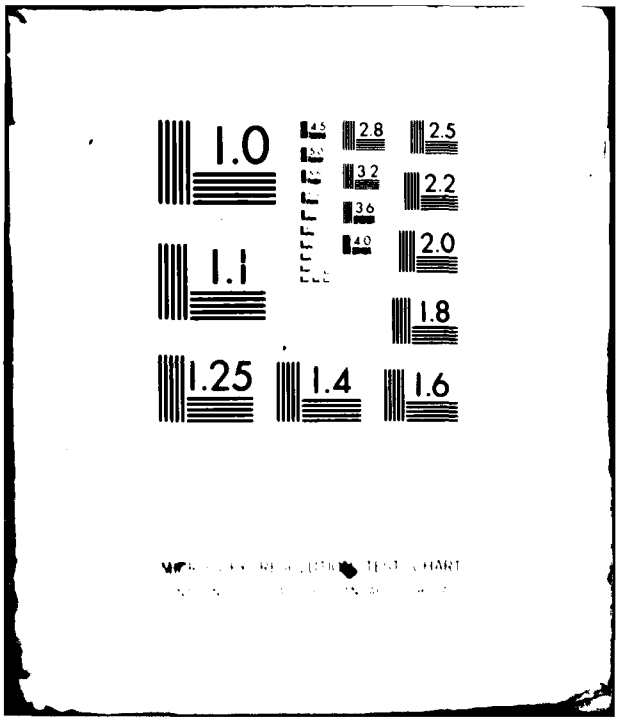
1.0
1.1
1.25
1.4
1.6
1.8
2.0
2.2
2.5
2.8
3.2
3.6
4.0
4.5

NAVAIR

NUMERICAL STUDIES OF THE RADIATION CONDITION AT THE INLET OF A TRANSONIC COMPRESSOR BLADE ROW

William J. Rae and Gregory F. Homicz
Aerodynamic Research Department
Calspan Corporation
P.O. Box 400
Buffalo, New York 14225

April 1980

Final Report for Period 26 October 1978 - 25 February 1980
Contract No. N00019-78-C-0603

Prepared For:
NAVAL AIR SYSTEMS COMMAND
DEPARTMENT OF THE NAVY
WASHINGTON, DC 20361

UNCLASSIFIED

SECURITY CLASSIFICATION OF THIS PAGE (When Data Entered)

REPORT DOCUMENTATION PAGE	READ INSTRUCTIONS BEFORE COMPLETING FORM
1. REPORT NUMBER	2. GOVT ACCESSION NO. AD-A085978 (9)
3. RECIPIENT'S CATALOG NUMBER	
4. TITLE (and Subtitle) NUMERICAL STUDIES OF THE RADIATION CONDITION AT THE INLET OF A TRANSONIC COMPRESSOR BLADE ROW (6)	5. TYPE OF REPORT & PERIOD COVERED Final Report. 26 Oct 1978 — 25 Feb 1980
	6. PERFORMING ORG. REPORT NUMBER 6432-A-1
7. AUTHOR(s) William J. Rae and Gregory F. Homicz (1)	8. CONTRACT OR GRANT NUMBER(s) N00019-78-C-0603 (15) new
9. PERFORMING ORGANIZATION NAME AND ADDRESS Calspan Corporation Advanced Technology Center P. O. Box 400, Buffalo, New York 14225	10. PROGRAM ELEMENT, PROJECT, TASK AREA & WORK UNIT NUMBERS (12) 37
11. CONTROLLING OFFICE NAME AND ADDRESS Naval Air Systems Command (AIR-310) Department of the Navy Washington, D.C. 20361 (11)	12. REPORT DATE April 1980
	13. NUMBER OF PAGES 30
14. MONITORING AGENCY NAME & ADDRESS(if different from Controlling Office) (14) CALSPAN-6432-A-1	15. SECURITY CLASS. (of this report) Unclassified
	15a. DECLASSIFICATION/DOWNGRADING SCHEDULE

16. DISTRIBUTION STATEMENT (of this Report)

APPROVED FOR PUBLIC RELEASE:
DISTRIBUTION UNLIMITED

17. DISTRIBUTION STATEMENT (of the abstract entered in Block 20, if different from Report)

18. SUPPLEMENTARY NOTES

19. KEY WORDS (Continue on reverse side if necessary and identify by block number)

Turbomachinery
Compressors
Transonic Flow

20. ABSTRACT (Continue on reverse side if necessary and identify by block number)

Finite-difference calculations of the flow in a transonic compressor blade row were carried out, using a radiation boundary condition at a plane upstream of the blades. These results show essentially no difference from a comparable set that were done using a uniform-flow approximation as the inlet boundary condition.

DD FORM 1 JAN 73 1473 EDITION OF 1 NOV 65 IS OBSOLETE

UNCLASSIFIED

SECURITY CLASSIFICATION OF THIS PAGE (When Data Entered)

3 1 2 1 0

ACKNOWLEDGEMENT

The authors wish to express their thanks to their colleagues John A. Lordi and John R. Moselle for their contributions to the work reported here.

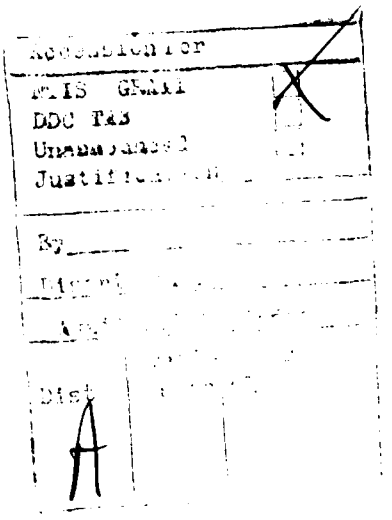

TABLE OF CONTENTS

LIST OF FIGURES

LIST OF TABLES

LIST OF SYMBOLS

a_∞	speed of sound far upstream
B	number of blades
C_a	axial projection of the chord
f	coordinate stretching factor
K, L, N	indices numbering the grid points in the $\bar{z}$, ζ , ρ directions
L_T	$2\pi r_T / B$
M_∞	u_∞ / a_∞
r, θ, x	cylindrical coordinates
u, v, w	perturbation velocity components in the $\bar{z}$, ρ , θ directions
$\bar{z}$	$\omega x / u_\infty$
γ	specific-heat ratio
Γ	circulation
$\Delta\phi(\rho)$	jump in potential across the trailing vortex sheet
ζ	$\theta - \bar{z}$
ρ	$\omega r / u_\infty$
ρ_∞	density far upstream
ϕ	velocity potential

Section 1
INTRODUCTION

The axial-flow fans and compressors used in aircraft gas-turbine propulsion systems frequently operate in a range where the flow over the blades is transonic. This situation arises at high values of the rotor angular velocity, where the resultant of the axial inlet speed of the gas and the rotational speed of the blades reaches the speed of sound at some station along the blade span. Under these circumstances, the moving blade experiences an inlet relative flow that is supersonic over the outer portion of the blade, and is subsonic near the hub. Shock waves are formed at the leading edge of the outer portion; these propagate upstream through the subsonic axial inlet flow, and are radiated away from the inlet itself.

The objective of the research reported here was to develop a method for incorporating these radiating waves in the numerical codes that are used for calculations of such flows. Calculations of this type have come into increasingly heavy use in recent years as a design tool, for screening candidate configurations. However, the calculation methods used at present ignore the effects due to the radiating waves, and assume instead that the flow at the inlet is uniform, and adequately described by the two-dimensional flow approximations at any radial location.

The adequacy of these approximations has been the subject of considerable study in recent years, especially because of the transonic nature of the flow. If, for example, the wave pattern radiated by the blades is estimated by the two-dimensional simple-wave model,[1,2] then the flow has

1. Rae, W.J. and Lordi, J.A., "A Study of Inlet Conditions for Three-Dimensional Transonic Compressor Flows", Calspan Report No. XE-6129-A-4 (June 1978).

2. Fink, M.R. "Shock Wave Behavior in Transonic Compressor Noise Generation", Trans ASME 93 (D) Journal of Engineering for Power No. 4 (October 1971) 397-403.

singular behavior at the sonic circle, i.e., at the radial station where the inlet relative Mach number is equal to one. Moreover, the distribution of inlet mass flow over the supersonic-inlet portion is conventionally taken as that given by the unique-incidence condition,[3] applied at each radius. This approximation neglects the radial interactions in the flow, and the resulting redistribution of mass flow that is known to occur.

In addition to the inadequacy of these approximations, it is reasonable to expect that the absence of a radiation condition would introduce numerical anomalies at the grid boundaries. The types of anomalous wave patterns expected are shown in Figure 1, which is a section through the blade row at a constant radius, outside the sonic circle. This figure, taken from a previous NAVAIR-sponsored study at Calspan,[1] suggests that waves which propagate upstream from the blade row would be reflected from the upstream grid boundary. As pointed out in Reference 1, previous attempts to calculate a supersonic-tip-speed case had encountered wavelike motions at the radial stations beyond the sonic circle. These motions were assumed to be caused by the lack of a radiation condition, and the objective of Reference 1, as well as the present work, was to apply a radiation condition in order to allow the waves to escape, and to learn from the resulting solutions how to simplify the procedure.

The approach that was followed in Reference 1 was to use the linear-theory formulation of the radiation condition, in conjunction with a computer code which solves the three-dimensional transonic flow in the nonlinear small-disturbance approximation.[4,5] The two solutions were matched along a plane

3. Lichtfuss, H.J. and Starken, H. "Supersonic Cascade Flow", pp. 37-149 of Progress in Aerospace Sciences Vol. 15 ed. by D. Kuchemann Pergamon Press, New York (1974).

4. Rae, W.J., "Computer Program for Relaxation Solutions of the Non-Linear Small-Disturbance Equations for Transonic Flow in an Axial Compressor Blade Row", AFOSR-TR-78-0855, (April 1978).

5. Rae, W.J. "Calculations of Three-Dimensional Transonic Compressor Flow Fields By A Relaxation Method" Journal of Energy 1 pp. 284-296 (1977).

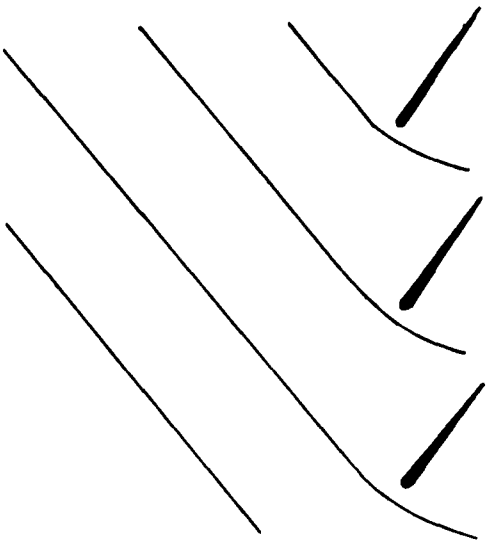

a.) WITHOUT REFLECTION

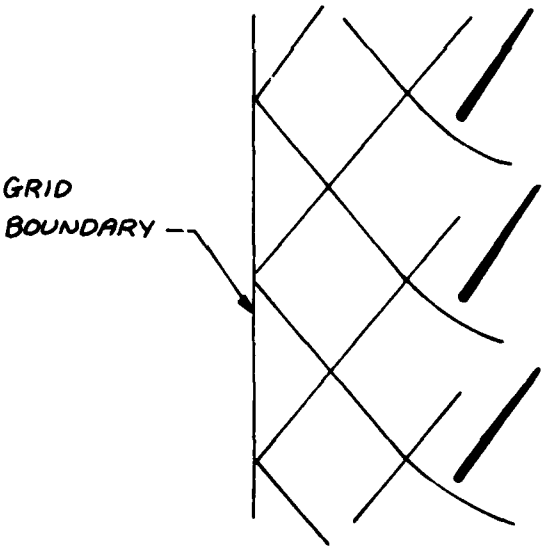

b.) WITH REFLECTION

FIGURE 1 WAVE PATTERNS EXPECTED

located a chord length or so upstream of the blade row; the numerical solution, at a given stage in the iterations, was used to calculate the amplitude coefficients in the Fourier-Bessel series representation of the outgoing waves in the linear theory. The velocity field derived from this series was then used as the boundary value for the next step of the numerical solution, and the process was repeated at regular intervals.

In Reference 1, the case chosen for application of this technique was a heavily loaded rotor with a relative Mach number of 1.3 at the tip. A series of attempts to calculate this flow, using the uniform-inlet boundary conditions, had led to solutions in which wavelike disturbances propagated back and forth through the flow. It was expected that introduction of the radiation condition would remove these wavelike oscillations. However, it did not; many attempts (reported in Reference 1) were made, with adjustments in the frequency of applying the radiation condition, but none of these succeeded in removing the waves. The work of Reference 1 concluded with the speculation that the case attempted was too difficult a test for the method, in that the blades were quite heavily loaded, and the initial flowfield too filled with steep waves.

Accordingly, the present investigation was undertaken, in which a new calculation was started from the very beginning. The blade geometry and operating conditions were chosen so as to have relatively modest values of the loading and Mach number. For this case, the procedure described above did lead to a converged solution.

However, the calculation was then repeated with the uniform-inlet boundary condition, in order to verify that the radiation condition was the factor responsible for the convergence. It was found that this calculation also converged, and converged to essentially the same answer as that found using the radiation condition.

To explore the problem further, the heavily loaded case was then calculated again - once with the radiation condition and once with the

uniform-inlet condition. Both of these calculations were started from an initial condition of uniform flow, and both led to the same phenomenon observed in the earlier work, namely, a series of waves was found to oscillate back and forth in the flow field. The detailed distributions of these oscillations at any stage of the iteration process were virtually the same for either of the boundary conditions used at the inlet.

Thus the final conclusion reached is a negative one: for the calculation that converged, the use of a radiation condition led to results which differed negligibly from those found using the uniform-inlet condition. Toward the end of the work reported here, a similar conclusion was reached in a study done at the MIT Gas Turbine Laboratory (Reference 6), using essentially the same formulation of the radiation condition, in conjunction with a numerical code that solves the full Euler equations.

The steps followed in reaching this conclusion are outlined in the Sections below: Section 2 contains a brief review of the numerical method, including some improvements that were made in the basic non-linear small-disturbance program while Section 3 describes the present calculations. Section 4 contains a discussion of the conclusions reached.

This report relies heavily on Reference 1, and is intended to be read in conjunction with it. Much of the notation, blade-geometry description, and computer-program details mentioned here are taken directly from Reference 1; those details have not been repeated in this text.

---

6. Berenfeld, S., "A Study of Boundary Conditions for Transonic Compressor Flows", M Sc. Thesis, Massachusetts Institute of Technology (June 1979).

The departure from periodicity was most noticeable in the second derivatives of the potential, especially when evaluated along the periodic boundaries [illegible] and [illegible]. This discrepancy was traced to the finite-difference formulas used to evaluate the second streamwise derivative at subsonic points. In the notation of Reference 4, the difference of the values of this derivative on the two periodic boundaries is proportional to the following

$$\phi_{\cdot\cdot} \quad \phi_{\cdot\cdot} \quad \cdots \quad \phi_{\cdot} \quad \phi_{\cdot\cdot\cdot} \quad \cdots \quad \phi_{\cdot} \quad \phi_{\cdot\cdot\cdot} \quad \cdots \quad \phi_{\cdot} \quad \phi_{\cdot\cdot\cdot}$$

$$\phi_{\cdot} \quad \cdots \quad \phi_{\cdot} \quad \cdots \quad \phi_{\cdot} \quad \phi_{\cdot}$$

NUMERICAL RESULT

, 5° INCIDENCE

LINEAR THEORY
ORIGINAL COMPUTER CODE
REVISED COMPUTER CODE

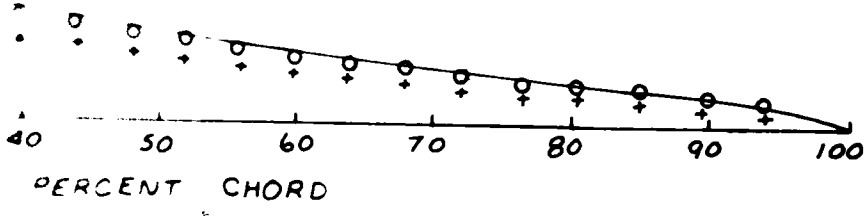

After Reference 4 was published, it was found that an extended form of the Thomas algorithm could be used, in which the periodic boundary conditions are enforced at every stage of the relaxation process, rather than being approached only as the solution converges. This extended form is described in Reference 9.

The details of the method are as follows: the grid points along the line being relaxed are numbered L = 1, 2, 3, ..., LMX; the difference equation has the form of a three-term recurrence relation:

$$A^L \phi^{L+1} + B^L \phi^L + C^L \phi^{L-1} = D^L \qquad L = 2, 3, \ldots, \quad LMX-1$$

where ϕ is the velocity potential, and the coefficients A^L, ..., D^L are known quantities at each value of L. The periodicity condition to be enforced upstream and downstream of the blades is

$$\phi' = \phi^{LMX} + \epsilon \Delta\phi$$

where $\epsilon = 0$ upstream of the blades, $\epsilon = 1$ downstream of the blades, and $\Delta\phi$ is the potential jump at the trailing edge.

The extended Thomas algorithm is implemented as follows: let

$$E(1) = 0 \ , \quad F(1) = 0 \ , \quad S(1) = 1$$

Then calculate

$$\left.\begin{aligned} E(L) &= A^L / [C^L E(L-1) + B^L] \\ F(L) &= [D^L - C^L F(L-1)] / [C^L E(L-1) + B^L] \\ S(L) &= -S(L-1) C^L E(L-1) / [C^L E(L-1) + B^L] \end{aligned}\right\} \quad L = 2, 3, \ldots, LMX$$

... and Walsh, J.L., The Theory of Splines and Their Applications, Academic Press, New York (1967) pp. 14-16.

Next, set

$$T(LMX) = 1 \quad , \quad V(LMX) = 0$$

and calculate

$$\left.\begin{aligned} T(L) &= E(L)\,T(L+1) + S(L) \\ V(L) &= E(L)\,V(L+1) + F(L) \end{aligned}\right\} \quad L = LMX-1,\ LMX-2,\ \ldots,\ 2$$

Then the potential at LMX is given by

$$\phi^{LMX} = \frac{-A^{LMX}[V(2) - \epsilon\Delta\phi] - C^{LMX}V(LMX-1) + D^{LMX}}{A^{LMX}T(2) + C^{LMX}T(LMX-1) + B^{LMX}}$$

Once this is known, the other values of LMX are found from the recursion relations:

$$\phi^{L} = E(L)\,\phi^{L+1} + F(L) + S(L)\,\phi^{LMX}, \quad L = 2,3,\ldots,LMX-1$$

$$\phi' = \phi^{LMX} + \epsilon\Delta\phi$$

At points on the blade, the normal Thomas algorithm is used, as before, by setting S, T, and V equal to zero.

Correction Form

The accuracy of the solution can be improved by using the "correction" form of the algorithm, i.e., on each iteration the change in the velocity potential is calculated:

$$C \equiv \overset{+}{\phi} - \phi$$

rather than the new value of the potential itself, $\overset{+}{\phi}$. This form minimizes the arithmetic problems that might arise from taking small differences of large numbers.

Exit-Plane Mach Number

The final change made in the relaxation method deals with the Mach number variation at the downstream edge of the grid. At that location, the velocity component ϕ_ξ is constrained to equal a certain constant, dictated by the requirement of mass-flow conservation. In the previous version of the program, this requirement was met by setting the potential values at the downstream edge of the grid equal to the value corresponding to a parabola through the two stations just upstream, and having the required slope. The revision incorporated in the present work is to set the velocity equal to the desired value at the next-to-last station, and to use this velocity in solving for the potential there. The potential at the last station is then found by a linear extrapolation, using the desired slope. A similar procedure was followed by Collins and Krupp.[10]

10. Collins, D.J., and Krupp, J.A., "Experimental and Theoretical Investigations in Two-Dimensional Transonic Flow", AIAA Journal 12 (1974) pp. 771-778.

Section 3
RESULTS OF PRESENT CALCULATIONS

Blade-Row Geometry

As noted in the Introduction, the case chosen for the previous work was felt to be too stringent a test of the radiation condition, because of the high degree of loading and because the initial solution that was used already contained steep wavelike disturbances. Accordingly, the blade geometry and operating conditions for the present calculations were carefully chosen so as to avoid these problems. Flat-plate blades were used, in order to eliminate blade thickness as a possible source of choking, and the blades were twisted so as to present a constant angle of incidence of six degrees to the relative inlet flow. This incidence was sufficient to insure subsonic flow over most of the region downstream of the blades, thus minimizing wave reflection at the downstream edge of the grid as a mechanism for instability in the calculations. The blade row had 30 blades, with a hub/tip radius ratio of 0.75 and a solidity C_a / L_T equal to 0.5. The axial Mach number was set equal to 0.5, and the rotational Mach number at the tip was 0.980, giving a distribution of inlet relative Mach number that varied from 0.889 at the hub to 1.100 at the tip.

The grid had 60 points in the axial direction, 20 in the blade-to-blade direction, and 10 radially. The grid extended from two axial chords upstream of the leading edge to two axial chords downstream of the trailing edge, and was stretched, as described in Reference 4, to concentrate points near midchord. This grid had the optimum grid size ratio for shock-wave capturing at mid span (see Reference 4).

Iteration Sequence

The Fourier-Bessel series was calculated using 11 terms in the m -series (m = 0 through 10) and 10 terms in the k -series (k = 1 through 10). On the first run, the quantities K_{mBk}, ϕ_{mBk}, and N_{mBk}(see Section 4

of Reference 1) were calculated and stored on tape. These values are shown in Table 1, where the dotted line separates the modes that propagate (above the line) from those that are damped (below the line). The calculations then proceeded through a series of sixteen radial iterations, each of which used 60 axial iterations. Thus the solution at each grid point was iterated 960 times. The fifth axial grid station, lying at 0.9752 axial chordlengths upstream of the leading-edge plane, was chosen as the matching plane. For the first 60 iterations (i.e., for the first radial sweep) uniform-flow conditions were imposed at the inlet, and thereafter the Fourier-Bessel series was used, with the amplitude coefficients A_{mBk} re-evaluated every 60 iterations (i.e., prior to every radial iteration). The angle of incidence and the relaxation factors used were increased gradually: incidence of 2° for the first 240 iterations, 4° for the next 60, and 6° thereafter, while the relaxation factors (for supersonic and subsonic points) were both taken as 0.2 for the first 120 iterations, 0.5 for the next 240, and 0.8 thereafter. An attempt to raise the subsonic relaxation factor to 1.2, starting at the 601st iteration, led to a divergent solution.

The convergence of the solution can be seen in the history of the local Mach number at a fixed point. Figure 3 shows this quantity at $\zeta = 0$, $x/C_a = 0.0126$, $\rho = 1.7419$. This point is located on the suction side, just downstream of the leading edge, and at a radius where the inlet relative Mach number is 1.0043. Thus it is in a region of peak acceleration. It is clear that the solution has essentially converged, at this stage of the iterations. Another measure of the convergence is the average residual, which after 960 iterations had decreased to 4.2% of the sum of the absolute values of the five terms in the finite-difference equation. Previous experience with this program indicates that further reductions of the residuals would require many more iterations, but would yield insignificant changes in the velocity distributions.

The amplitude coefficients in the Fourier-Bessel series did not show the same degree of convergence. Some of these coefficients were changing only slightly at the end of the calculation, but others were still growing; in

TABLE 1. Eigenvalues for the Fourier-Bessel Series (Twisted Flat-Plate Case)

K	KMBK/PHMBK/NORMBK, M = 0, 10										
	1.251D+01	3.252D+01	6.318D+01	9.364D+01	1.240D+02	1.543D+02	1.846D+02	2.148D+02	2.450D+02	2.752D+02	3.054D+02
1	8.709D-01	3.543D-03	2.805D-06	2.500D-08	9.043D-13	4.448D-16	2.074D-19	9.294D-23	4.042D-26	1.716D-29	7.144D-33
	1.055D-01	5.871D-02	3.781D-02	2.916D-02	2.422D-02	2.096D-02	1.861D-02	1.683D-02	1.542D-02	1.428D-02	1.333D-02
	2.515D+01	3.809D+01	7.058D+01	1.020D+02	1.331D+02	1.641D+02	1.949D+02	2.257D+02	2.563D+02	2.870D+02	3.176D+02
2	9.329D-01	3.499D-01	4.290D-03	1.269D-05	4.215D-08	3.052D-11	3.373D-14	3.243D-17	2.804D-20	2.230D-23	1.657D-26
	7.695D-02	8.419D-02	4.674D-02	3.820D-02	3.207D-02	2.795D-02	2.495D-02	2.265D-02	2.082D-02	1.932D-02	1.807D-02
	3.771D+01	4.323D+01	7.583D+01	1.081D+02	1.399D+02	1.711D+02	2.024D+02	2.335D+02	2.645D+02	2.954D+02	3.263D+02
3	9.547D-01	3.960D-02	1.589D-01	2.086D-03	1.030D-05	4.871D-08	6.754D-11	1.174D-13	1.722D-16	2.209D-19	2.546D-22
	6.352D-02	5.850D-02	5.464D-02	4.040D-02	3.413D-02	2.990D-02	2.678D-02	2.438D-02	2.246D-02	2.089D-02	1.956D-02
	5.028D+01	5.133D+01	8.020D+01	1.134D+02	1.456D+02	1.773D+02	2.089D+02	2.403D+02	2.715D+02	3.027D+02	3.338D+02
4	9.658D-01	8.699D-02	5.593D-01	6.356D-02	8.871D-04	5.862D-06	4.329D-08	7.337D-11	1.750D-13	3.478D-16	5.968D-19
	5.532D-02	4.637D-02	5.815D-02	4.256D-02	3.518D-02	3.093D-02	2.779D-02	2.536D-02	2.341D-02	2.180D-02	2.044D-02
	6.284D+01	6.111D+01	8.615D+01	1.179D+02	1.509D+02	1.830D+02	2.148D+02	2.465D+02	2.780D+02	3.094D+02	3.407D+02
5	9.725D-01	3.128D+00	-4.923D-01	4.299D-01	2.431D-02	3.601D-04	2.858D-06	3.788D-08	5.699D-11	1.725D-13	4.330D-16
	4.964D-02	1.308D-01	4.555D-02	4.855D-02	3.616D-02	3.156D-02	2.843D-02	2.600D-02	2.403D-02	2.241D-02	2.104D-02
	7.540D+01	7.178D+01	9.382D+01	1.227D+02	1.556D+02	1.883D+02	2.204D+02	2.523D+02	2.841D+02	3.156D+02	3.471D+02
6	9.771D-01	2.365D+00	1.198D-01	3.495D-01	2.305D-01	9.204D-03	1.430D-04	1.315D-06	9.941D-09	3.657D-11	1.334D-13
	4.542D-02	9.142D-02	3.614D-02	4.024D-02	3.935D-02	3.210D-02	2.887D-02	2.644D-02	2.448D-02	2.285D-02	2.147D-02
	8.797D+01	8.300D+01	1.026D+02	1.291D+02	1.600D+02	1.933D+02	2.268D+02	2.579D+02	2.898D+02	3.216D+02	3.532D+02
7	9.803D-01	2.704D-01	-5.720D-01	-1.514D+00	5.671D-01	1.050D-01	3.486D-03	5.620D-05	5.656D-07	2.163D-08	2.079D-11
	4.212D-02	3.366D-02	3.755D-02	6.026D-02	4.168D-02	3.352D-02	2.921D-02	2.676D-02	2.481D-02	2.318D-02	2.181D-02
	1.005D+02	9.456D+01	1.121D+02	1.366D+02	1.655D+02	1.977D+02	2.306D+02	2.632D+02	2.953D+02	3.272D+02	3.591D+02
8	9.827D-01	-2.464D+00	1.625D+00	-2.254D-01	-2.217D-02	4.502D-01	4.401D-02	1.324D-03	2.192D-05	2.537D-07	2.451D-08
	3.945D-02	7.998D-02	5.748D-02	3.113D-02	3.146D-02	3.747D-02	2.987D-02	2.701D-02	2.506D-02	2.344D-02	2.207D-02
	1.131D+02	1.063D+02	1.222D+02	1.449D+02	1.721D+02	2.024D+02	2.354D+02	2.683D+02	3.006D+02	3.327D+02	3.647D+02
9	9.846D-01	1.343D-01	-4.575D+00	-3.261D-01	-2.450D+01	4.367D-01	2.653D-01	1.777D-02	5.037D-04	8.529D-06	1.228D-07
	3.723D-02	2.839D-02	1.319D-01	2.974D-02	7.035D-01	3.319D-02	3.230D-02	2.735D-02	2.525D-02	2.364D-02	2.228D-02
	1.257D+02	1.193D+02	1.327D+02	1.538D+02	1.795D+02	2.083D+02	2.398D+02	2.731D+02	3.057D+02	3.380D+02	3.701D+02
10	9.862D-01	2.473D+00	-2.622D+00	-2.208D+00	-7.876D-01	-5.033D-01	5.689D-01	1.329D-01	7.061D-03	1.919D-04	3.297D-06
	3.534D-02	7.076D-02	7.449D-02	6.449D-02	3.412D-02	3.074D-02	3.422D-02	2.854D-02	2.546D-02	2.380D-02	2.244D-02

FIGURE 3 LOCAL MACH NUMBER AT L=1, K=20, N=6

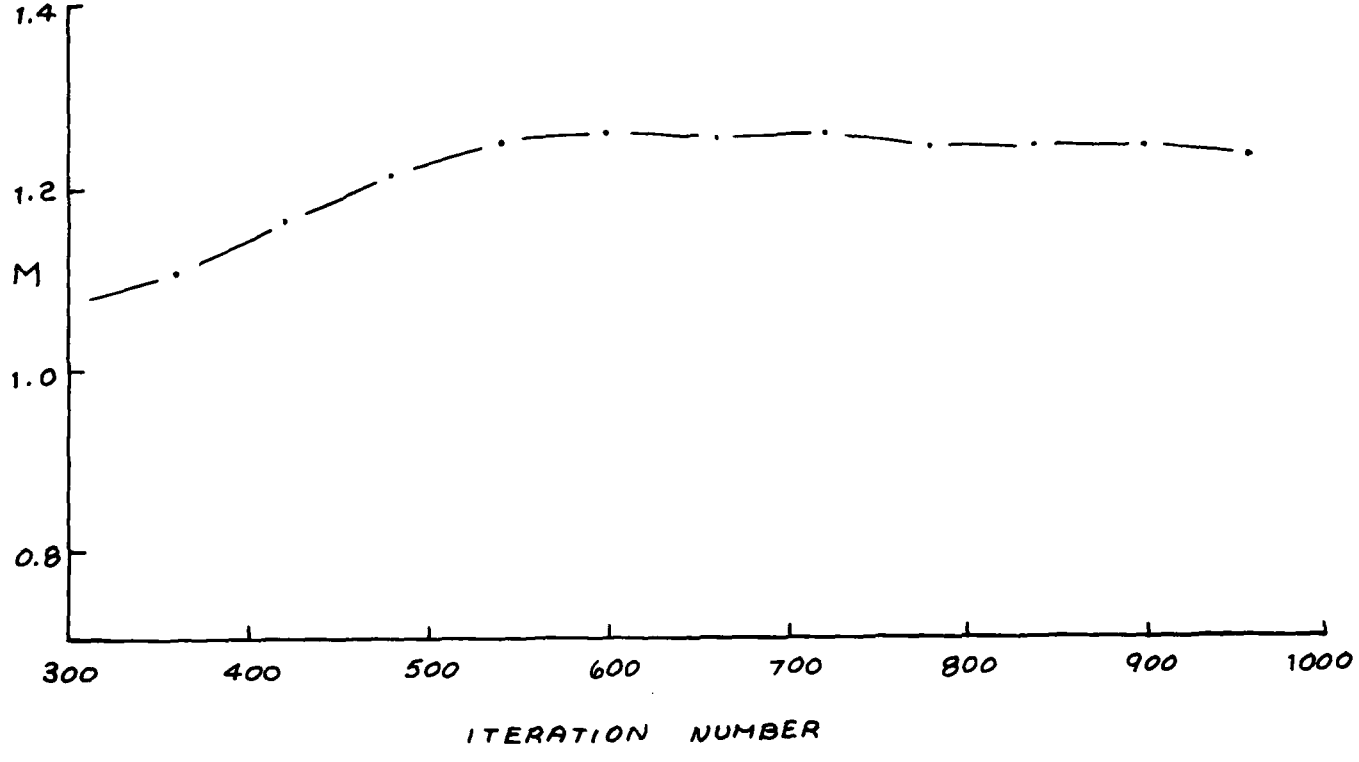

particular, the constant term A_{oo} was still increasing. Table 2 shows the values of these coefficients used for the final 60 iterations. It is obvious that only the first few modes are present in the numerical data.

Sonic-line contours from the final iteration are shown in Figure 4; the significance of these results is discussed at greater length in Section 4.

Check Runs

After the solution described above was completed, several shorter runs were made, in order to verify that the radiation condition was in fact the critical element that had allowed convergence. In these shorter runs, the final 120 iterations were repeated, without the radiation condition, and using several values of the relaxation factors. These runs produced the surprising result that the solutions were virtually identical to that described above. It is possible that 120 iterations is insufficient to allow instabilities in the flow to develop, but it seems unlikely, especially in view of the high degree of identity between solutions with and without the radiation conditions: there were no differences between the two solutions, to three-figure accuracy. The fact that the detailed history of these two solutions was so nearly identical prompted several checks of the program logic, to verify that the radiation condition was actually being used.

At this point, it was decided to repeat the calculation of the highly loaded case done in the previous study. This was done to find out whether the changes that had been made to the program might have removed some previously undetected errors that were causing the oscillations in the solution.

Thus, the 23-blade heavily-loaded-rotor case described in the previous report was repeated, starting from the very beginning, i.e., from a uniform-flow condition throughout the flow field. Relaxation factors of 0.8 were used at all points, subsonic and supersonic, throughout the entire series of iterations. To start the calculation, two radial sweeps were done, each with

TABLE 2

Fourier-Bessel Coefficients Used for the Final 60 Iterations

(Twisted Flat-Plate Case)

K	AMK REAL/AMK IMAGINARY, M = 0, 10									
0	4.312E-03									
1	3.070E-04	-5.579E-04	1.652E-05	-2.003E-07	-2.018E-08	-1.264E-08	-2.681E-09	-3.581E-10	-1.167E-09	1.320E-09	5.568E-11
		4.831E-04	4.705E-06	-9.522E-07	-4.363E-08	3.330E-10	-3.257E-10	-2.529E-09	-6.918E-10	4.334E-10	-6.347E-10
2	-6.917E-05	-1.755E-04	1.466E-06	1.940E-07	2.048E-08	-5.727E-09	-1.595E-09	-3.114E-10	-1.060E-09	1.128E-09	8.082E-11
		-1.051E-05	1.168E-05	-3.339E-07	-2.956E-08	-2.239E-09	-3.682E-10	-2.358E-09	-4.970E-10	3.406E-10	-5.529E-10
3	2.469E-05	1.631E-05	-3.830E-06	6.932E-08	2.891E-08	-1.614E-09	-9.243E-10	-2.675E-10	-9.832E-10	8.737E-10	8.432E-11
		-7.407E-06	4.316E-06	1.171E-07	-4.687E-09	-1.204E-09	-4.452E-11	-1.916E-09	-3.114E-10	1.643E-10	-4.373E-10
4	-9.462E-06	-1.793E-07	-1.304E-06	-1.092E-07	8.980E-09	-2.073E-09	-7.974E-10	-2.105E-10	-9.309E-10	8.348E-10	7.464E-11
		1.332E-06	2.061E-10	8.487E-08	4.713E-09	5.368E-10	4.701E-10	-1.667E-09	-2.384E-10	5.515E-11	-3.501E-10
5	3.116E-06	-1.444E-06	-3.072E-07	-9.781E-08	-2.800E-09	-2.462E-09	-5.174E-10	-2.675E-12	-7.300E-10	7.703E-10	1.165E-10
		1.810E-06	-1.672E-07	5.950E-09	2.087E-09	5.852E-10	8.143E-10	-1.491E-09	-2.757E-10	3.236E-12	-3.161E-10
6	-1.299E-08	3.850E-07	-8.267E-08	-3.496E-08	-2.741E-09	-1.304E-09	-5.660E-10	2.489E-10	-5.608E-10	6.070E-10	7.796E-11
		-4.721E-07	-1.947E-08	-2.018E-08	-2.212E-09	-2.499E-10	4.353E-10	-1.339E-09	-3.171E-10	-1.910E-11	-2.898E-10
7	-1.329E-06	-1.454E-07	-2.437E-08	-3.190E-09	-1.628E-09	-7.138E-10	-8.298E-10	-1.099E-10	-5.375E-10	4.282E-10	-3.366E-11
		5.380E-07	7.821E-08	-9.150E-09	-3.018E-09	-7.188E-10	-2.199E-10	-1.107E-09	-2.441E-10	-2.278E-11	-2.443E-10
8	1.640E-06	3.666E-07	-6.872E-08	1.639E-09	-6.266E-10	-1.165E-09	-5.832E-10	-2.970E-10	-6.015E-10	4.472E-10	-3.728E-11
		-4.201E-07	-5.123E-08	-1.888E-09	-1.412E-09	-1.652E-10	1.250E-10	-9.783E-10	-1.227E-10	2.419E-11	-2.585E-10
9	-1.447E-06	-2.779E-07	4.103E-08	-9.220E-11	7.089E-10	-2.706E-11	-3.006E-10	1.933E-11	-5.445E-10	4.619E-10	2.469E-11
		-2.557E-07	-2.876E-08	2.719E-09	-2.912E-10	-4.040E-10	3.920E-10	-9.614E-10	-1.069E-10	3.417E-11	-2.801E-10
10	1.058E-06	2.769E-07	-1.991E-08	4.065E-09	2.176E-10	2.567E-10	-3.204E-10	-1.514E-11	-4.193E-10	3.938E-10	3.286E-11
		-3.688E-07	-1.036E-08	3.215E-10	5.541E-11	-2.868E-10	-4.216E-11	-8.829E-10	-1.594E-10	1.002E-11	-2.722E-10

MACH NUMBER CONTOURS AT ρ = 1.5241 (N=2)

INLET RELATIVE MACH NUMBER = 0.9115

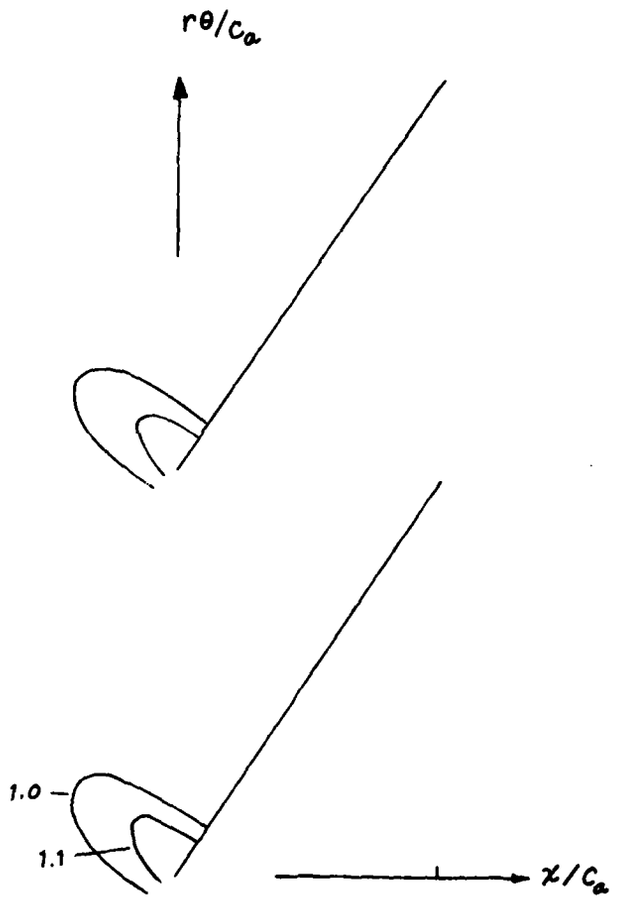

FIGURE 4a

MACH NUMBER CONTOURS AT ρ = 1.5786 (N = 3)

INLET RELATIVE MACH NUMBER = 0.9343

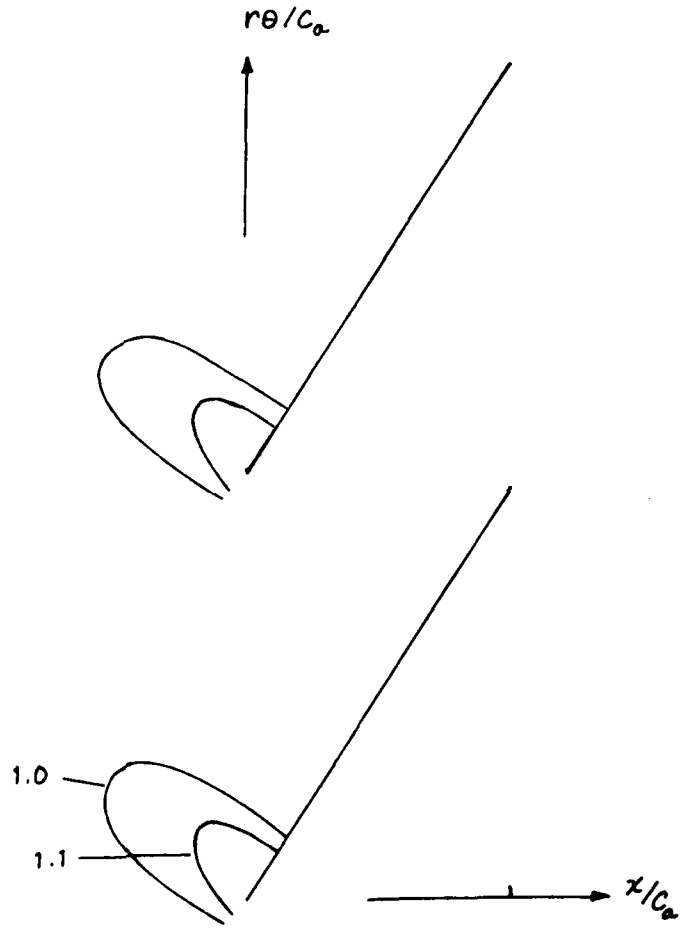

FIGURE 4b

MACH NUMBER CONTOURS AT β = 1.6330 (N = 4)

INLET RELATIVE MACH NUMBER = 0.9574

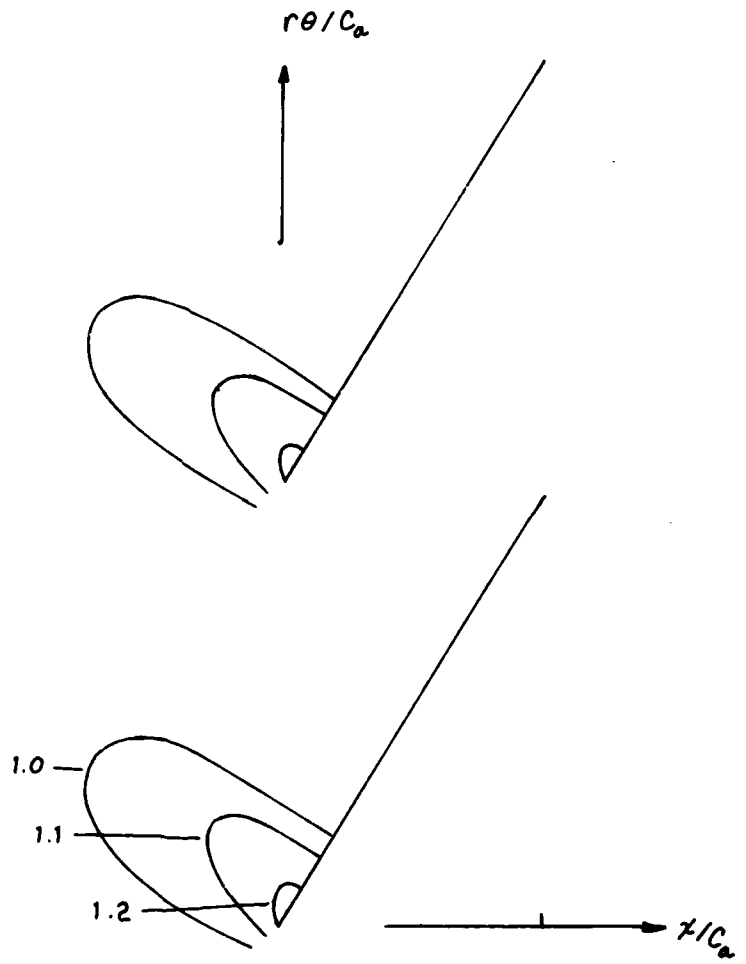

FIGURE 4c

MACH NUMBER CONTOURS AT $\rho = 1.6874$ (N=5)

INLET RELATIVE MACH NUMBER = 0.9807

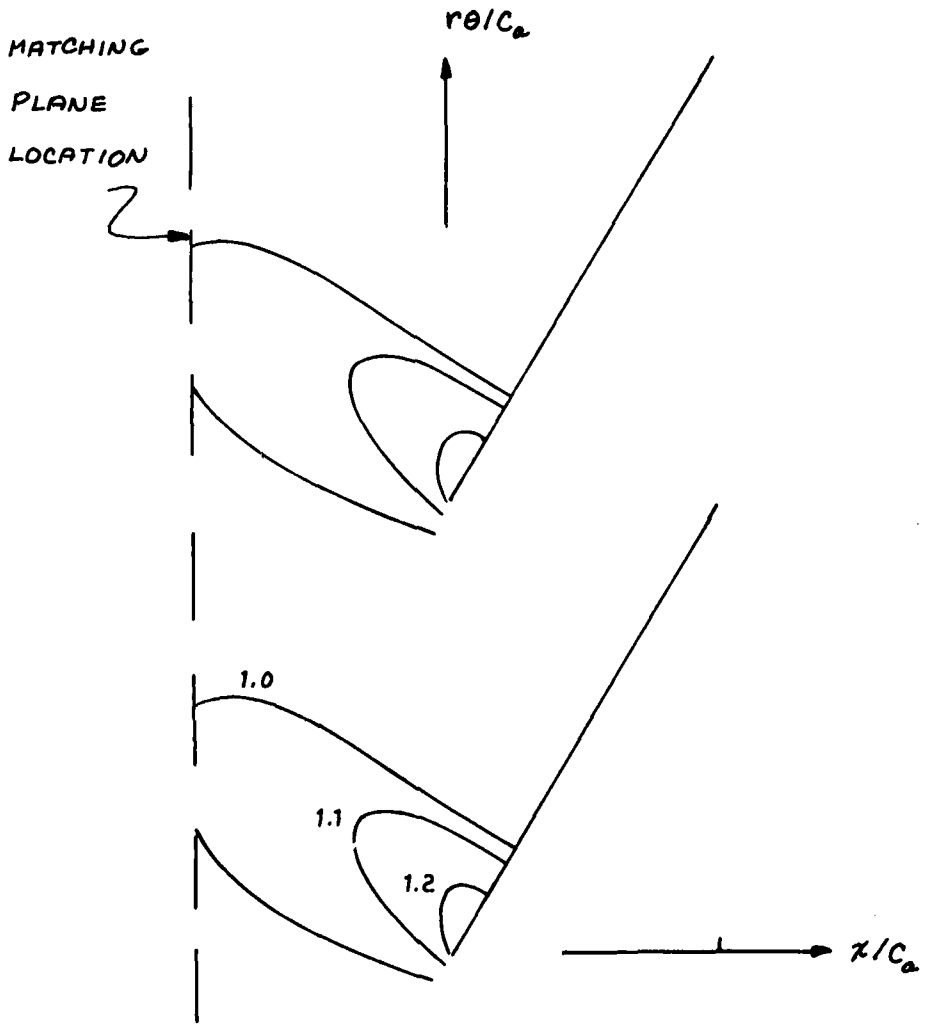

FIGURE 4d

MACH NUMBER CONTOURS AT ρ = 1.7419 (N=6)

INLET RELATIVE MACH NUMBER = 1.0043

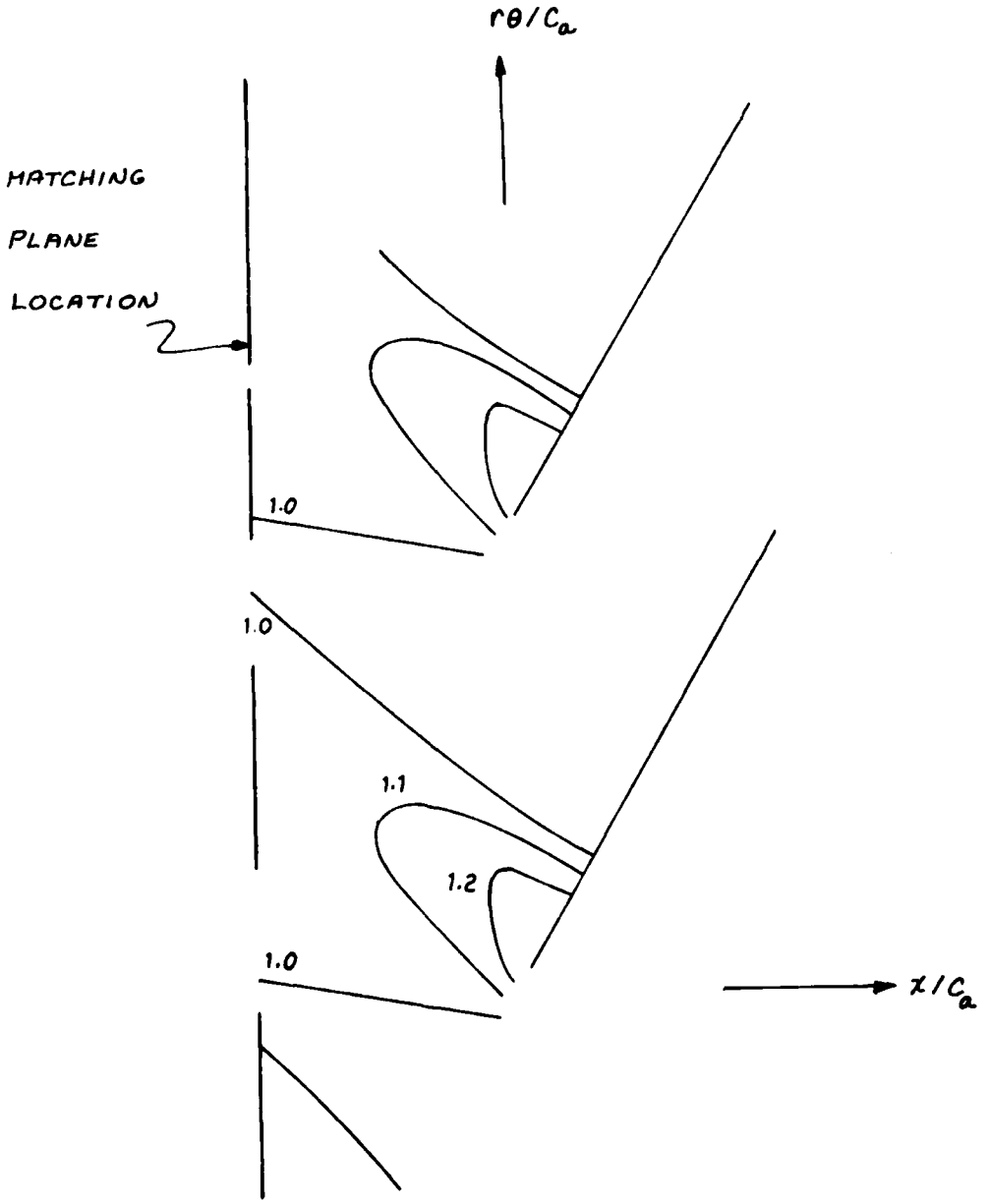

FIGURE 4e

MACH NUMBER CONTOURS AT ρ = 1.7963 (N=7)

INLET RELATIVE MACH NUMBER = 1.0279

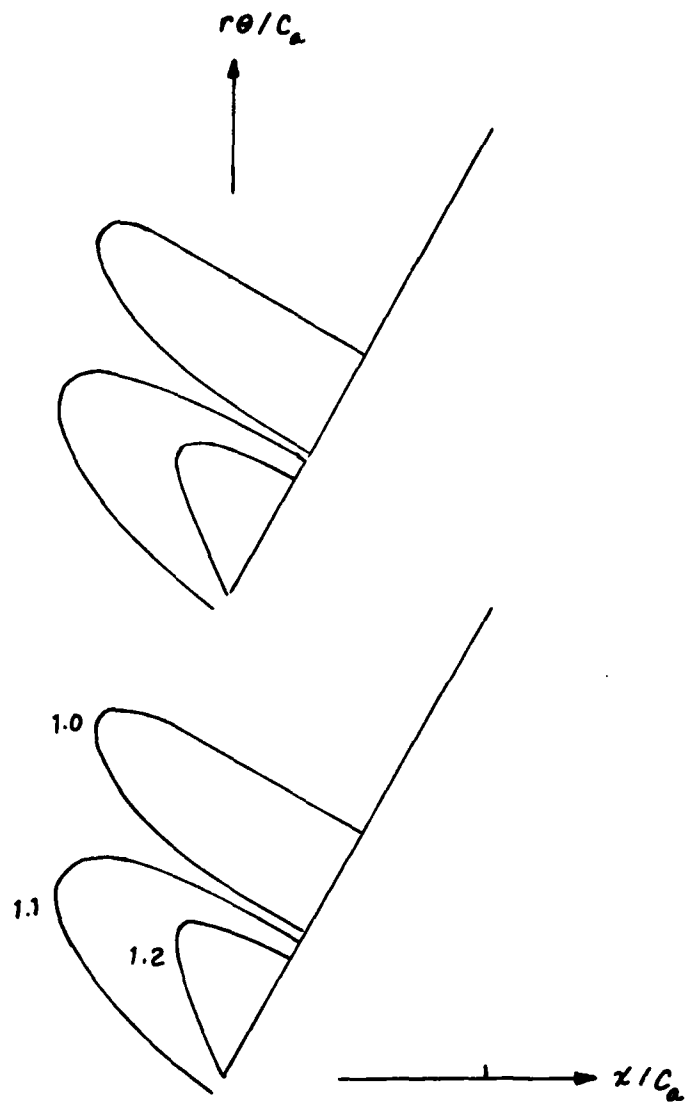

FIGURE 4f

MACH NUMBER CONTOURS AT $\rho = 1.8507$ ($N = \beta$)

INLET RELATIVE MACH NUMBER = 1.0518

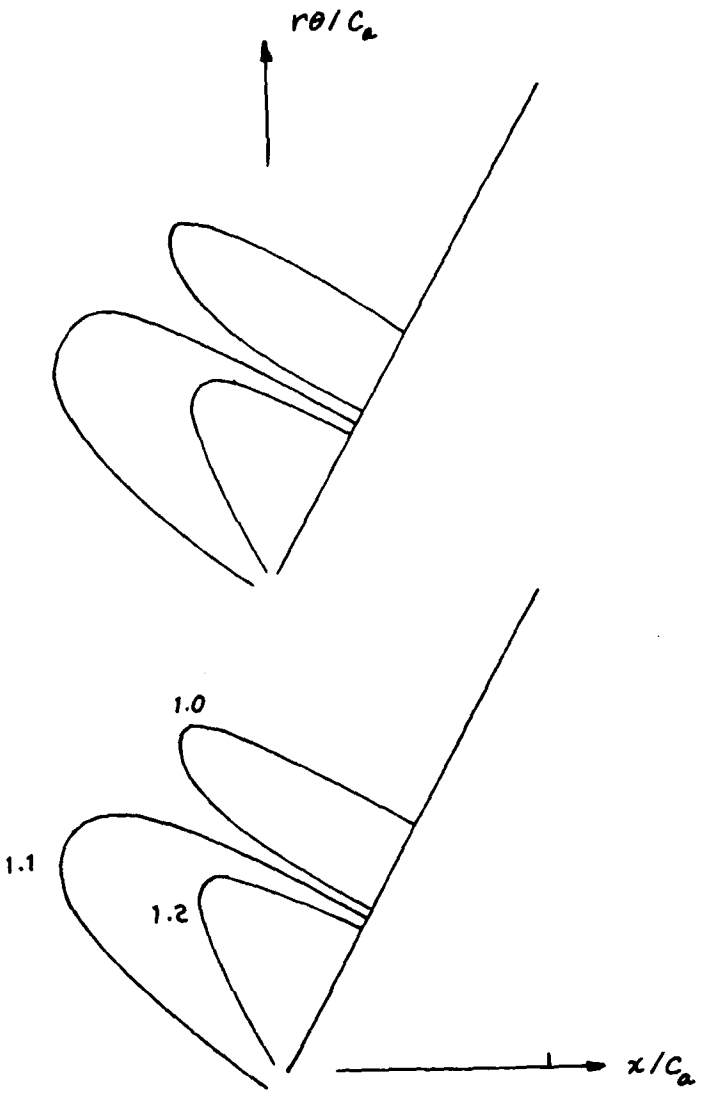

FIGURE 4g

MACH NUMBER CONTOURS AT ρ = 1.9052 (N=9)

INLET RELATIVE MACH NUMBER = 1.0758

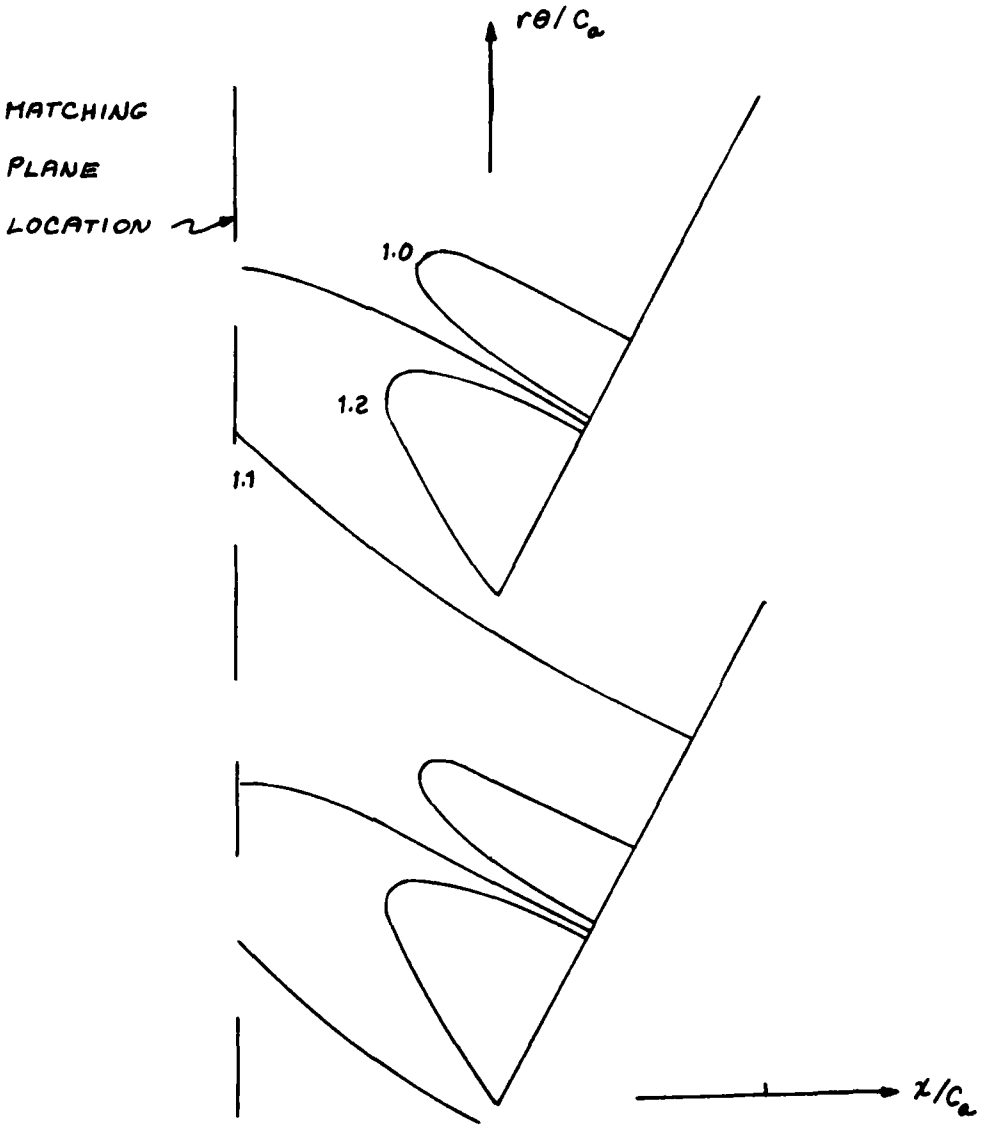

FIGURE 4h

60 axial sweeps, for a total of 120 updates of the solution at each grid point. Thereafter, this initial run was continued on two parallel paths - with the radiation condition and with the uniform-flow inlet condition. Both of these calculations were run for 10 further radial iterations, at 60 axial iterations each, bringing the total number of iterations to 720. The radiation condition was updated every 60 iterations.

Both of these solutions showed the same type of oscillatory behavior as that observed during the previous work.[1] Moreover, the oscillating time histories of the potential distribution calculated with the two inlet conditions were virtually identical to each other, iteration by iteration.

Section 4
CONCLUSIONS

The conclusion that emerges from these calculations is that the boundary conditions used at the inlet have a negligible effect on the flow field solution, at least for the set of conditions represented by the case which converged. This conclusion is in accord with the results of an independent study recently completed at the MIT Gas Turbine Laboratory.[6] While differing in details, the essential conclusion reached in that work is the same as that reached here.

The limits over which this conclusion applies are not established by the results of the present study, since only a single case has been run to convergence. For the case which did not converge, it is true that the inlet condition had no effect on the solution, but this leaves open the question whether such an effect was suppressed by the presence of the oscillating waves.

The original hypothesis on which this work was based was that the oscillations in the solution were caused by wave reflections from the upstream boundary. These reflections, in turn, were assumed to be generated by the imposition of the uniform-inlet conditions. The converged results from the twisted flat-plate case make it clear that the latter assumption is not always realized; the Mach-number contours in Figure 4 are not affected by the imposition of uniform-flow conditions at the matching plane. Thus the mechanism for generating oscillations in the solution is more complex; it may be dependent on the amplitude of the disturbances reaching the matching plane, on the relaxation factors being used, and on other sources, that are unknown at present.

Several aspects of the calculations reported here require further elaboration: the number of iterations used, the occurrence of supersonic outflow, and the schedule used for the relaxation factors.

Number of Iterations

The magnitude of the residuals remaining after 960 iterations (for the twisted flat-plate case described in Section 3) is somewhat larger than the standard usually considered acceptable for a finite-difference solution. However, it is also characteristic of line-relaxation methods that the short-wavelength errors decay very slowly. And while these errors may yield large values of the residual, they do not have a major effect on the gross flow field, nor do they lead to divergent behavior as the solution progresses. The general nature of line-relaxation methods indicates that these solutions were carried far enough to provide the required opportunity for the radiation condition to make its presence felt.

Supersonic Outflow

The angle of incidence used for the twisted flat-plate case was raised to six degrees in order to insure that the flow at the exit plane would be subsonic. As noted earlier, this was done to remove wave reflections from the downstream edge of the grid as a possible source of oscillatory behavior. The Mach number distributions reached on the 960th iteration fell just short of this goal, in that the exit-plane Mach number at the radial station next to the outer wall was 1.003. However, there was no evidence of wave reflections in this vicinity.

Relaxation-Factor Schedule

One noteworthy difference between the twisted flat-plate case and the heavily-loaded-rotor case is the schedule of relaxation factors used. These were varied from 0.2 to 0.8 in the former case, but were set equal to 0.8 throughout the latter case. This raises the question whether the latter case might have converged, if the relaxation factors had been increased gradually.

Finally, it is appropriate to return to consideration of the longer-range goal of this research, namely to shed light on the nature of the subsonic/supersonic transition that occurs near the sonic circle. The twisted flat-plate solution does not offer a great deal of information concerning this question. Specifically, the sonic-line contours found in the vicinity of the sonic circle do not suggest any simple interpretation; they are not aligned at any recognizable Mach angle, and the radial variation of their structure is not resolved adequately by the grid size employed here. Thus such questions as shock-wave refraction and mass flow diversion in the vicinity of the sonic circle must await further calculations, done with greater resolution.

REFERENCES

1. Rae, W.J. and Lordi, J.A., "A Study of Inlet Conditions for Three-Dimensional Transonic Compressor Flows", Calspan Report No. XE-6129-A-4 (June 1978).

2. Fink, M.R., "Shock Wave Behavior in Transonic Compressor Noise Generation", Trans ASME 93 (D) Journal of Engineering for Power No. 4 (October 1971) 397-403.

3. Lichtfuss, H.J. and Starken, H., "Supersonic Cascade Flow", pp. 37-149 of Progress in Aerospace Sciences Vol. 15 ed. by D. Kuchemann, Pergamon Press, New York (1974).

4. Rae, W.J., "Computer Program for Relaxation Solutions of the Non-Linear Small-Disturbance Equations for Transonic Flow in an Axial Compressor Blade Row", AFOSR-TR-78-0855, (April 1978).

5. Rae, W.J., "Calculations of Three-Dimensional Transonic Compressor Flow Fields By A Relaxation Method", Journal of Energy 1 pp. 284-296 (1977).

6. Berenfeld, S., "A Study of Boundary Conditions for Transonic Compressor Flows", M Sc. Thesis, Massachusetts Institute of Technology (June 1979).

7. Homicz, G.F. and Lordi, J.A., "Three-Dimensional Lifting-Surface Theory For An Annular Blade Row" ASME Paper 79-GT-182 (March 1979).

8. Richtmeyer, R.D., and Morton, K.W., Difference Methods for Initial-Value Problems, 2nd Edition, Interscience Publishers, New York (1967) Section 8.5.

9. Ahlberg, J.H., Nilson, E.N., and Walsh, J.L., The Theory of Splines and Their Applications, Academic Press, New York (1967) pp. 14-16.

10. Collins, D.J., and Krupp, J.A., "Experimental and Theoretical Investigations in Two-Dimensional Transonic Flow", AIAA Journal 12 (1974) pp. 771-778.

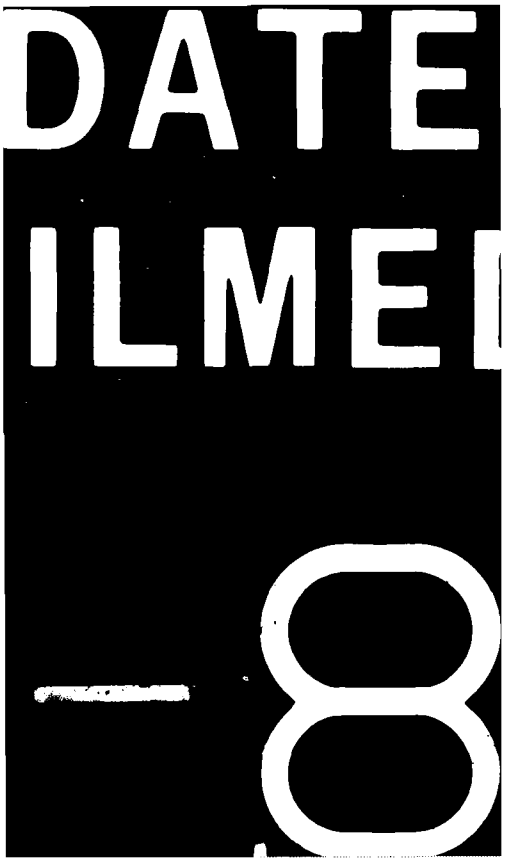
DATE
ILME
8